MOLECULAR ENDOCRINOLOGY

Contrasting Skeletal Phenotypes in Mice with an Identical Mutation Targeted to Thyroid Hormone Receptor {alpha}1 or {beta}

Patrick J. O'Shea, J. H. Duncan Bassett, Srividya Sriskantharajah, Hao Ying, Sheue-yann Cheng and Graham R. Williams

Mol. Endocrinol. 2005 19:3045-3059 originally published online Jul 28, 2005; , doi: 10.1210/me.2005-0224

0888-8809/05/$15.00/0
Printed in U.S.A.

Molecular Endocrinology 19(12):3045–3059

doi: 10.1210/me.2005-0224

Contrasting Skeletal Phenotypes in Mice with an Identical Mutation Targeted to Thyroid Hormone Receptor α1 or β

Patrick J. O'Shea, J. H. Duncan Bassett, Srividya Sriskantharajah, Hao Ying, Sheue-yann Cheng, and Graham R. Williams

Molecular Endocrinology Group (P.J.O., J.H.D.B, S.S., G.R.W.), Division of Medicine and Medical Research Council Clinical Sciences Centre, Imperial College London, Hammersmith Campus, London, W12 0NN, United Kingdom; and Gene Regulation Section (H.Y., S.-y.C.), Laboratory of Molecular Biology, National Cancer Institute, National Institutes of Health, Bethesda, Maryland 20892-4264

Thyroid hormone (T_3) regulates bone turnover and mineralization in adults and is essential for skeletal development. Surprisingly, we identified a phenotype of skeletal thyrotoxicosis in T_3 receptor β^{PV} (TRβ^{PV}) mice in which a targeted frameshift mutation in TRβ results in resistance to thyroid hormone. To characterize mechanisms underlying thyroid hormone action in bone, we analyzed skeletal development in TRα1^{PV} mice in which the same PV mutation was targeted to TRα1. In contrast to TRβ^{PV} mice, TRα1^{PV} mutants exhibited skeletal hypothyroidism with delayed endochondral and intramembranous ossification, severe postnatal growth retardation, diminished trabecular bone mineralization, reduced cortical bone deposition, and delayed closure of the skull sutures. Skeletal hypothyroidism in TRα1^{PV} mutants was accompanied by impaired GH receptor and IGF-I receptor expression and signaling in the growth plate, whereas GH receptor and IGF-I receptor expression and signaling were increased in TRβ^{PV} mice. These data indicate that GH receptor and IGF-I receptor are physiological targets for T_3 action in bone *in vivo*. The divergent phenotypes observed in TRα1^{PV} and TRβ^{PV} mice arise because the pituitary gland is a TRβ-responsive tissue, whereas bone is TRα responsive. These studies provide a new understanding of the complex relationship between central and peripheral thyroid status. (*Molecular Endocrinology* 19: 3045–3059, 2005)

THE ACTIONS OF THYROID hormone (T_3) are mediated mainly by nuclear T_3 receptors (TRs), which act as ligand-inducible transcription factors (1). Several TRα and TRβ isoforms are expressed in temporospatial patterns during development and in differing ratios in adult tissues (1–3). In the skeleton, TRs are expressed in growth plate chondrocytes, osteoblasts, and bone marrow stromal cells, and T_3 is essential for skeletal development, linear growth, and bone mineralization (4, 5). Childhood hypothyroidism causes growth arrest, delayed skeletal maturation, and epiphyseal dysgenesis, and T_4 replacement induces catch-up growth (6). Autosomal dominant resistance to thyroid hormone (RTH), which results from mutant TRβ proteins, also impairs skeletal development causing short stature and bone dysplasias (7, 8). Childhood thyrotoxicosis accelerates growth and advances bone age but induces short stature due to premature fusion of the growth plates. In severe cases, craniosynostosis can result from early closure of the skull sutures and may be associated with neurological deficits (9). Thus, euthyroidism is essential for normal bone development, and the skeleton is exquisitely sensitive to changes in thyroid status.

RTH is characterized by reduced responsiveness of target tissues to circulating T_4 and T_3. At the level of the hypothalamic-pituitary-thyroid axis this results in the classical biochemical features of RTH, in which negative feedback control of TSH production and secretion is impaired. The resulting inappropriately high levels of TSH drive increased T_4 and T_3 production, and a new equilibrium set point of high circulating concentrations of T_4 and T_3 with elevated levels of TSH is established. Mutations in the *THRB* gene cause RTH and result in the expression of mutant TRβ proteins that are unable to respond normally to T_3, usually because of reduced binding affinity for T_3 or reduced transcriptional activation capabilities. The mutant TRβ proteins also interfere with the actions of normally expressed wild-type TRα and β and thus act as dominant-negative antagonists that disrupt transcription of

First Published Online July 28, 2005

Abbreviations: ALSKO, Acid-labile subunit knockout; E17.5, embryonic d 17.5; FGFR, fibroblast growth factor receptor; GHR, GH receptor; IGF-1R, IGF-I receptor; LID, liver-specific IGF-I knockout; HZ, hypertrophic zone; P1, postnatal d 1; PZ, proliferative zone; RTH, resistance to thyroid hormone; RZ, reserve zone; STAT, signal transducer and activator of transcription; TR, T_3 receptor.

***Molecular Endocrinology* is published monthly by The Endocrine Society (http://www.endo-society.org), the foremost professional society serving the endocrine community.**

T_3-regulated genes (10). The clinical syndrome of RTH is variable, resulting from both the direct effects of the mutant receptors and the consequences of elevated thyroid hormone concentrations. In addition, the differing ratios of TRα and TRβ proteins that are expressed in individual tissues further complicate the syndrome. In tissues such as the heart, in which TRα predominates, the presence of tachycardia in RTH is likely to be due to the effects of elevated thyroid hormone levels acting via TRα. In contrast, in tissues such as the liver, in which TRβ predominates, the presence of hypercholesterolemia in RTH may result from a combination of local tissue hypothyroidism and the direct dominant-negative actions of mutant TRβ proteins in hepatocytes. Thus, the spectrum of clinical features in RTH is broad and can include reduced weight, cardiac disease, hypercholesterolemia, tachycardia, hearing loss, attention-deficit hyperactivity disorder, decreased IQ, and dyslexia (10–12). This complex spectrum reflects the presence of thyrotoxicosis in some T_3-target tissues but evidence of hypothyroidism in others.

A wide variety of bone phenotypes has been described in RTH, and this is probably because objective studies of the skeleton and growth are available in only a small minority of patients. Features include stippled epiphyses with scattered calcification in the growth plate, high bone turnover osteoporosis and fracture, reduced bone density, craniosynostosis, and various defects of facial bone and vertebral development (7). Growth retardation and short stature have been estimated to occur in 26% of patients with variably delayed bone age in up to 47% (7, 8), although bone age has also been shown to be advanced by more than 2 SDS in two families, and lesser degrees of advancement have also been documented (7).

In a previous study, we characterized skeletal development in mutant mice with a PV mutation targeted to the TRβ gene locus (13). The PV mutation was derived from a patient with severe RTH and consists of a C insertion at codon 448, which produces a frameshift of the carboxyl-terminal 14 amino acids of TRβ1. The mutant TRβ^{PV} protein cannot bind T_3, fails to transactivate T_3 target genes *in vitro*, and is a potent dominant-negative antagonist (14). TRβ^{PV} mice have very high levels of circulating T_4, T_3, and TSH (14), and we showed they display a phenotype of skeletal thyrotoxicosis (13). We also demonstrated that TRα1 mRNA is expressed at 12-fold higher concentrations than TRβ1 in bone, suggesting that the phenotype of skeletal hyperthyroidism in TRβ^{PV} mice results from increased T_3 levels acting via TRα1 (13). To investigate this hypothesis and determine whether TRα1 is functionally predominant in bone, we studied mice carrying the PV mutation targeted to TRα1 (15). The mutant TR$\alpha1^{PV}$ protein also acts as a potent dominant-negative antagonist that interferes with transcriptional activities of the wild-type TRα and TRβ receptors (15). In keeping with other mice with dominant-negative RTH mutations in TRα1 (11, 16), heterozygous TR$\alpha1^{PV/+}$ mice display only a modest degree of thyroid failure. There were small increases in TSH (1.7-fold) and T_3 (1.15-fold) levels in TR$\alpha1^{PV/+}$ mice, but no change in circulating T_4 concentrations, and the homozygous mutation was lethal (15). Characterization of bone development in biochemically euthyroid TR$\alpha1^{PV/+}$ mice, therefore, enabled us to investigate mechanisms of T_3 action in bone and determine whether TRα1 is the major functional TR expressed in the skeleton.

RESULTS

TR$\alpha1^{PV/+}$ Mice Exhibit Delayed Ossification and Postnatal Growth Retardation

Analysis of bone lengths in TR$\alpha1^{PV/+}$ mice revealed severe and persistent postnatal linear growth impairment (Fig. 1). No sexually dimorphic influences of the TR$\alpha1^{PV}$ mutation on bone growth or development were observed. TR$\alpha1^{PV/+}$ tibias were 15–25% shorter than tibias from wild-type littermates at all postnatal ages examined. In contrast, no difference was observed between embryonic d 17.5 (E17.5) and postnatal d 1 (P1) wild-type and TR$\alpha1^{PV/+}$ mice. TR$\alpha1^{PV/+}$

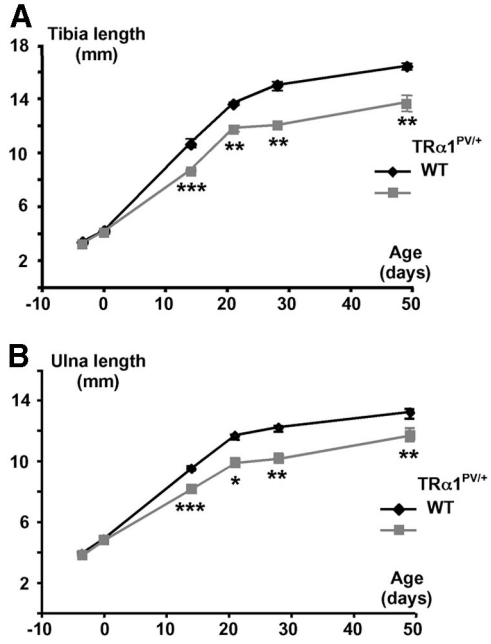

Fig. 1. Growth of Wild-Type (WT) and TR$\alpha1^{PV/+}$ Mice

A, *Graph* showing mean tibia lengths (mm) in mice between E17.5 (2.5 d before birth) and 7 wk. B, *Graph* showing mean ulna lengths (mm) in mice between E17.5 and 7 wk. Significance of differences between WT and TR$\alpha1^{PV/+}$ at each age was calculated by Student's *t* test: *, $P < 0.05$; **, $P < 0.01$; ***, $P < 0.001$. Total numbers of animals examined per group were: WT E17.5, n = 6; neonate P1, n = 3; P14, n = 6; P21, n = 4; P28, n = 4; P49, n = 10; TR$\alpha1^{PV/+}$ E17.5, n = 7; neonate P1, n = 12; P14, n = 8; P21, n = 4; P28, n = 4; P49, n = 8.

ulnas were also markedly shorter than wild-type (12–14% reduction), although the magnitude of growth impairment was less than in the tibia (Fig. 1). This degree of postnatal growth impairment in TRα1$^{PV/+}$ long bones was much more severe than documented in TR$\beta^{PV/+}$ and TR$\beta^{PV/PV}$ mice (13).

Analysis of skeletal preparations from E17.5 and P1 TRα1$^{PV/+}$ mice confirmed that bone lengths in mutant mice did not differ from wild type before birth, and the appearance of rib cages and vertebrae from wild-type and TRα1$^{PV/+}$ mice was similar (Fig. 2A). In these preparations, alizarin red stained ossified bone pink and alcian blue 8GX stained cartilage blue. Nevertheless, analysis of limbs in E17.5 mice revealed a small delay in endochondral ossification in the ulna and radius of the forelimb and in the tibia and fibula of the hindlimb that was evident in all TRα1$^{PV/+}$ mice examined (reduced alizarin red staining in these regions in TRα1$^{PV/+}$ mice [(n = 7) compared with wild-type (n = 6), *arrowed* in Fig. 2A]. Similar findings were present in neonatal mice (wild-type n = 3; TRα1$^{PV/+}$ n = 12; data not shown). These observations are in contrast with findings in TR$\beta^{PV/PV}$ mice, in which E17.5 and P1 skeletons displayed advanced endochondral ossification and were larger than wild-type littermates (13). Examination of the skull in E17.5 and neonatal mice revealed further differences between wild-type and TRα1$^{PV/+}$ mice. There was no difference in anterior-posterior and biparietal skull dimensions, but the fontanelles in TRα1$^{PV/+}$ mice were larger and cranial sutures wider than in wild-type littermates [E17.5: 37.9 $\pm$ 2.5 *vs.* 20.8 $\pm$ 0.9 ($P < 0.001$); P1: 9.5 $\pm$ 0.8 *vs.* 4.3 $\pm$ 1.2 ($P < 0.05$), area of open fontanelles and sutures expressed as percentage of total skull area in TRα1$^{PV/+}$ *vs.* wild-type mice], indicating delayed fontanelle closure and suture fusion (Fig. 2). Intramembranous bone deposited in frontal and parietal bones of the TRα1$^{PV/+}$ skull was also more porous and stained less intensely (Fig. 2B). These data demonstrate normal growth dimension, but markedly delayed intramembranous ossification of the skull in TRα1$^{PV/+}$ mice and contrast with findings in TR$\beta^{PV/PV}$ mice, in which advanced ossification of the skull with craniosynostosis was demonstrated (13).

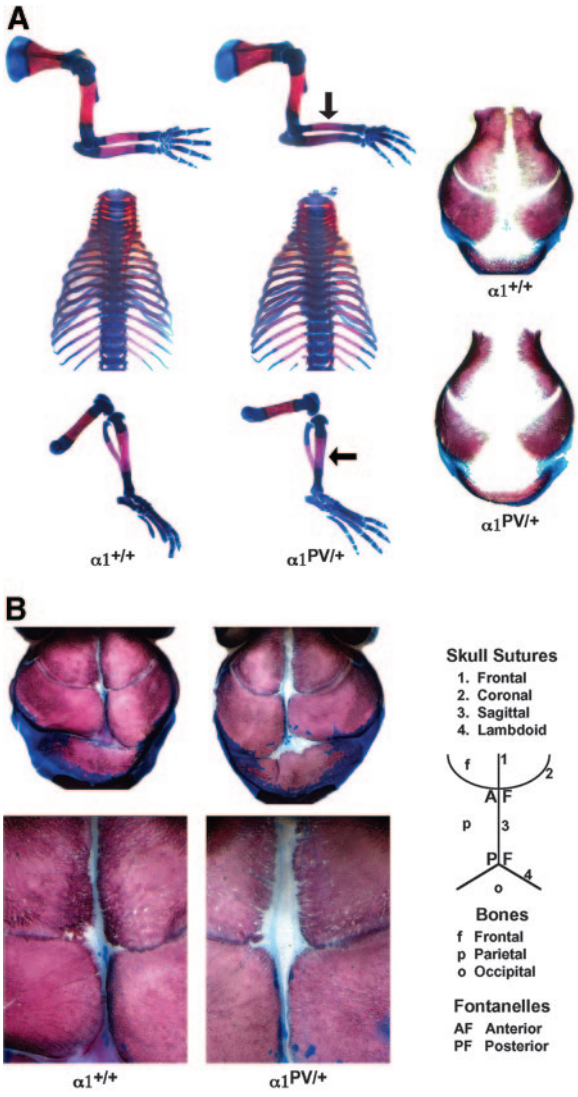

Fig. 2. Skeletal Preparations from Wild-Type ($\alpha 1^{+/+}$) and TRα1$^{PV/+}$ Mice Stained with Alizarin Red (Bone) and Alcian Blue 8GX (Cartilage)

A, E17.5 mice, limbs ×10, rib cages ×7.5, and skulls ×11 magnification. *Arrows* indicate distal fore- and hindlimbs in TRα1$^{PV/+}$ mice and show reduced alizarin red staining in mutants compared with wild-type littermates. B, Neonatal mice, skulls ×11 and ×30 magnification. Anatomy of the skull sutures, bones, and fontanelles is shown in the *adjacent diagram*.

Postnatal linear growth in TRα1$^{PV/+}$ and TR$\beta^{PV/PV}$ mice was examined in detail (Fig. 3). Tibias from TRα1$^{PV/+}$ mice were 15%, 17%, 20%, and 16% shorter than wild type at ages 2, 3, 4, and 7 wk, respectively, whereas tibias from TR$\beta^{PV/PV}$ mice were 11% shorter at 2 wk and only 2% shorter at 4 wk reflecting the accelerated growth spurt between these ages in TR$\beta^{PV/PV}$ mice (13). Growth impairment in TRα1$^{PV/+}$ mice was accompanied by reduced ossification of the secondary tibial epiphyses, a finding not seen in TR$\beta^{PV/PV}$ mice, but which persisted in TRα1$^{PV/+}$ mice at 3 and 4 wk. Furthermore, hindlimb paws from TRα1$^{PV/+}$ mice at 3 and 7 wk revealed persistently impaired endochondral bone formation with delayed formation of secondary ossification centers in metatarsal bones at 2 wk and the presence of open metatarsal growth plates at 7 wk (Fig. 3). In contrast, epiphyseal ossification and metacarpal and metatarsal growth plate closure was advanced in 3 wk-old TR$\beta^{PV/PV}$ mice (13). These data indicate that postnatal linear growth impairment in TRα1$^{PV/+}$ mice was associated with delayed endochondral ossification, whereas in TR$\beta^{PV/PV}$ mice it resulted from advanced bone development.

Endochondral ossification in the proximal tibia was analyzed in histological studies in TRα1$^{PV/+}$ mice (Fig. 4). In wild-type mice the proximal tibia secondary os-

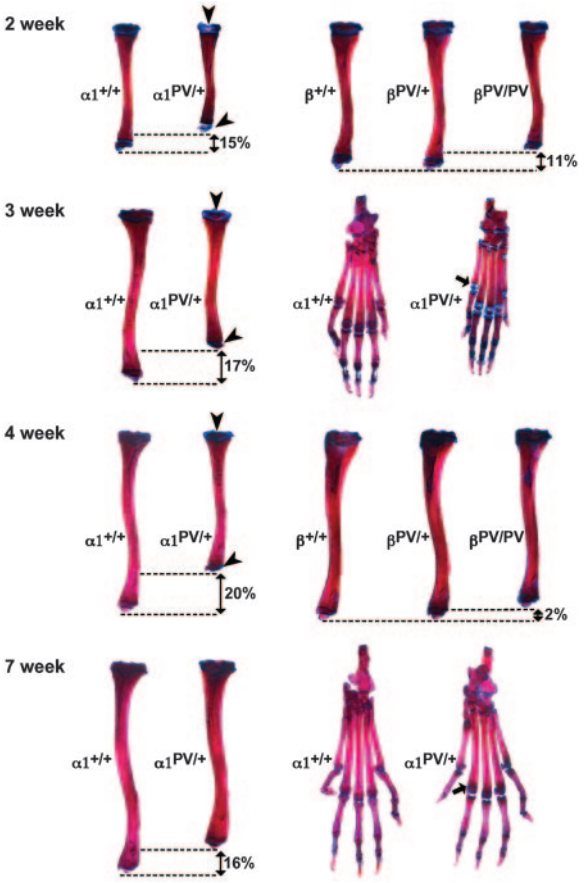

Fig. 3. Skeletal Preparations from Wild-Type ($\alpha1^{+/+}$) and TR$\alpha1^{PV/+}$ Mice Aged 2, 3, 4, and 7 wk and from Wild-Type ($\beta^{+/+}$), Heterozygote ($\beta^{PV/+}$), and Homozygous Mutant TR$\beta^{PV/PV}$ Mice Aged 2 and 4 wk

Tibias are shown at all ages and hindlimb paws are shown at ages 3 and 7 wk for $\alpha1^{+/+}$ and $\alpha1^{PV/+}$ mice. Preparations were stained with alizarin red (bone) and alcian blue (cartilage). Magnification ×6 in all cases. *Arrowheads* in panels showing tibias from 2-, 3-, and 4-wk mice indicate delayed formation of proximal and distal secondary ossification centers in $\alpha1^{PV/+}$ mice. *Arrows* in panels showing hindlimb paws indicate delayed formation of secondary epiphyses (3 wk) and persistence of the growth plate (7 wk) in metatarsals of $\alpha1^{PV/+}$ mice. The percentage differences in lengths of TR$\alpha1^{PV/+}$ tibias compared with wild-type littermates, and TR$\beta^{PV/PV}$ tibias compared with wild-type and heterozygote TR$\beta^{PV/+}$ littermates, are shown.

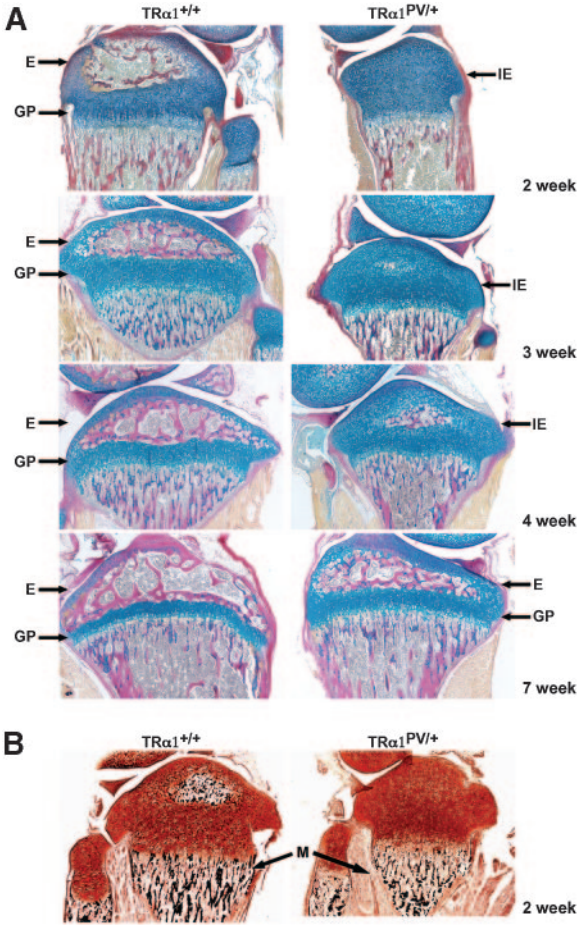

Fig. 4. Histological Sections of the Upper Tibia from Wild-Type (TR$\alpha1^{+/+}$) and TR$\alpha1^{PV/+}$ Mice

A, Sections of the upper tibia from 2-, 3-, 4-, and 7-wk wild type (TR$\alpha1^{+/+}$) and TR$\alpha1^{PV/+}$ mice (×50 magnification) stained with alcian blue (growth plate cartilage in blue) and van Gieson (bone osteoid in red). The proximal tibia secondary ossification center of the epiphysis (E) and the growth plate (GP) regions are shown along with immature epiphyses (IE). B, Undecalcified sections of the upper tibia and fibula from 2-wk wild type (TR$\alpha1^{+/+}$) and TR$\alpha1^{PV/+}$ mice (×50 magnification) stained with von Kossa (calcified bone in *black*) and neutral *red* counterstain. The metaphysis (M) *below* the growth plate is shown and denotes the region in which calcified trabecular bone is stained *black*. The epiphysis in the wild type (TR$\alpha1^{+/+}$) contains calcified bone stained *black*, whereas no von Kossa staining is seen in this region in TR$\alpha1^{PV/+}$ mice.

sification center was already established with formation of bone trabeculae within the epiphysis at 2 wk. Between 2 and 7 wk there was progressive narrowing of the growth plate with increased epiphyseal trabecular bone deposition as endochondral ossification and bone maturation continued. In contrast, in TR$\alpha1^{PV/+}$ mice endochondral ossification was markedly delayed. TR$\alpha1^{PV/+}$ tibias were smaller in all dimensions, and development of the secondary ossification center was initiated at 3 wk, a time at which this process was well advanced in wild-type littermates. Formation of an organized growth plate, and subsequent growth plate narrowing during the progression of endochondral ossification, was also markedly delayed. The histological features in 7-wk TR$\alpha1^{PV/+}$ mice were similar to those in 3- to 4-wk wild-type mice, indicating that endochondral ossification was delayed by up to 4 wk in mutants (Fig. 4A). Delayed endochondral ossification in TR$\alpha1^{PV/+}$ mice was associated with reduced deposition of calcified trabecular bone, as evidenced by reduced von Kossa staining of undecalcified sections of the tibia in 2-wk-old mutants ($n = 3$) compared with wild type ($n = 3$) (Fig. 4B). In particular, mineralization

of trabecular bone in the secondary epiphysis in wild-type mice was already established by 2 wk of age, whereas in TRα1$^{PV/+}$ mice, staining in this region was absent. A smaller reduction in von Kossa staining was evident in trabecular bone in the region of the metaphysis in TRα1$^{PV/+}$ mice. In addition, cortical bone deposition in the tibial diaphysis was reduced by approximately 50% in 2-wk TRα1$^{PV/+}$ mice compared with wild-type littermates (Fig. 5). These data demonstrate that postnatal growth impairment in TRα1$^{PV/+}$ mice is associated with a 3- to 4-wk delay in bone formation, reduced trabecular bone mineralization, and impaired cortical bone deposition. The findings contrast with those in TR$\beta^{PV/PV}$ mice, in which advanced ossification and increased trabecular bone mineralization were evident (13).

To investigate mechanisms underlying delayed ossification in TRα1$^{PV/+}$ mice, measurements of specific regions in the growth plate were performed (Fig. 6). Histological studies enabled the reserve (RZ), proliferative (PZ), and hypertrophic (HZ) zones of growth plates to be identified (13, 17–19). *In situ* hybridization was performed to determine the expression of collagen II, a marker of proliferating chondrocytes (20), and allow measurement of growth plate dimensions (Fig. 6A). Between 2 and 4 wk there was progressive narrowing of the growth plate in wild-type mice that was due to the normal proportionate narrowing in each of the RZ, PZ, and HZ regions (Fig. 6B). The growth plate continued to narrow in wild-type mice between 4 and 7 wk, but at a slower rate than in younger animals reflecting growth plate maturation and its imminent quiescence as linear growth tails off toward adulthood (Fig. 6C). In TRα1$^{PV/+}$ mice, measurement of specific regions of the growth plate were not possible until animals reached 7 wk of age because, before that time, formation of the proximal tibial growth plate was incomplete (Fig. 4). At 7 wk the growth plate in TRα1$^{PV/+}$ mice was significantly wider than in 7-wk wild-type littermates ($P < 0.001$) but did not differ in width when compared with growth plates from 4-wk wild-type mice. The finding that the width of the growth plate in 4-wk wild-type mice was similar to the width observed in 7-wk old TRα1$^{PV/+}$ mice suggested that endochondral ossification was delayed by about 3 wk in TRα1$^{PV/+}$ mice. Thus, comparisons of individual growth plate zones between 4-wk wild-type and 7-wk TRα1$^{PV/+}$ mice were made to investigate why ossification was delayed in TRα1$^{PV/+}$ mutants. These comparisons revealed that the PZ and HZ regions in TRα1$^{PV/+}$ mice were narrower than in wild-type (5% and 10%, respectively; $P < 0.05$) but the RZ width was similar to wild type (Fig. 6B). Taken together, these data confirm that endochondral ossification in TRα1$^{PV/+}$ mice is delayed by approximately 3–4 wk and suggest this delay is due to impaired transition of immature RZ chondrocytes into the PZ, resulting in proportionally reduced numbers or dimensions of proliferating and hypertrophic chondrocytes. The data contrast with findings in TR$\beta^{PV/PV}$ mice, in which disproportionate and accelerated narrowing of the PZ and HZ regions accounted for premature growth plate quiescence by 4 wk of age (13).

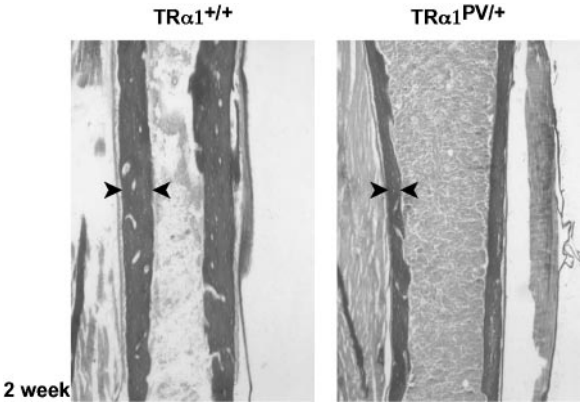

Fig. 5. Sections of the Midtibia Diaphysis from 2-wk-Old Wild-Type (TRα1$^{+/+}$) and TRα1$^{PV/+}$ mice ($\times$10 Magnification) Stained with van Gieson

Background shows nonspecific staining of bone marrow within the diaphysis cavity or skeletal muscle. The *arrowheads* indicate the width of cortical bone present in wild-type TRα1$^{+/+}$ and mutant TRα1$^{PV/+}$ littermates.

TRα1$^{PV/+}$ Mice Exhibit Skeletal Hypothyroidism

We previously identified that fibroblast growth factor receptor-1 (FGFR1) is a T_3-target gene in bone. Skeletal FGFR1 expression was reduced in TRα-null (TR$\alpha^{0/0}$) mice, which display a hypothyroid skeletal phenotype (19), but was increased in TR$\beta^{PV/PV}$ mice (13). In contrast, comparison of 3-wk-old wild-type mice with 7-wk-old TRα1$^{PV/+}$ mice (equivalent ages of growth plate maturation, Figs. 4 and 6) revealed that FGFR1 mRNA expression in both chondrocytes and osteoblasts was markedly reduced in TRα1$^{PV/+}$ mice (Fig. 7). These data demonstrate that TRα1$^{PV/+}$ mice display severe skeletal hypothyroidism.

GH and IGF-I Signaling in the Growth Plate Is Impaired in TRα1$^{PV/+}$ Mice, but Increased in TRβ^{PV} Mice

In view of the impaired transition of chondrocytes from RZ to PZ in TRα1$^{PV/+}$ mice, we investigated further by examining GH/IGF-I signaling in the growth plate. The GH/IGF-I pathway is initiated by GH, which activates the GH receptor (GHR) in growth plate chondrocytes. GH either acts directly on growth plate chondrocytes to regulate their proliferation and differentiation or stimulates local production of IGF-I, which subsequently acts in a paracrine manner to stimulate the IGF-I receptor (IGF-IR). IGF-I also exerts GH-independent actions on growth plate chondrocytes (21). GHR stimulation results in activation of a signaling cascade that involves signal transducer and activator of transcription (STAT)5 (22, 23), whereas stimulation of

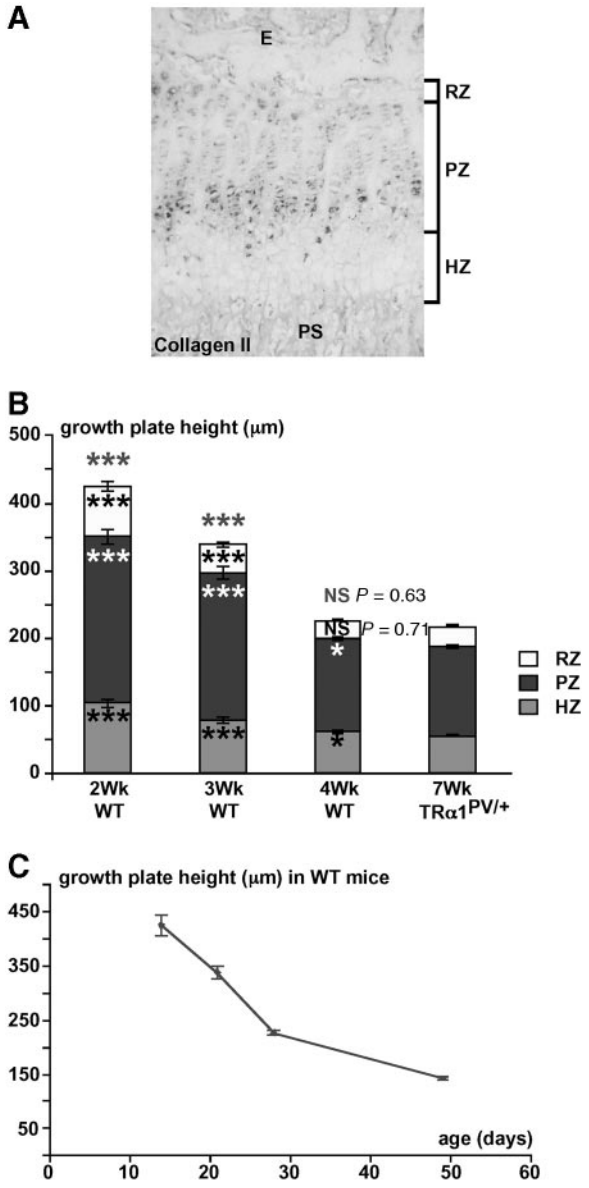

Fig. 6. Analysis of Growth Plate Dimensions in Wild-Type (WT) and TR$\alpha 1^{PV/+}$ Mice

A, *In situ* hybridization for collagen II expression in proliferative zone of the upper tibia growth plate of a 3-wk WT mouse (×200 magnification). RZs, PZs, and HZs of the growth plate are indicated along with the regions of the secondary epiphysis (E) and primary spongiosum (PS). B, *Graph* showing relative widths of the RZ, PZ, and HZ regions and total growth plate heights (RZ+PZ+HZ) of 2-, 3-, and 4-wk WT mice compared with 7-wk TR$\alpha 1^{PV/+}$ mice. Mean growth plate height and zone width measurements (μm) ± SEM were obtained from two to three animals per group (three to four differing levels of section examined for each growth plate) by taking four separate measurements across each growth plate section examined. Data were analyzed by Student's *t* test to determine the differences in width of the growth plate zones and the total growth plate height between 7-wk TR$\alpha 1^{PV/+}$ mice and WT animals aged 2, 3, and 4 wk. C, *Graph* showing the decline in total growth plate height (μm) ± SEM with age in WT mice aged between 2 and 7 wk (n = 3 per group). NS, Nonsignificant ($P = 0.63$; $P = 0.71$).

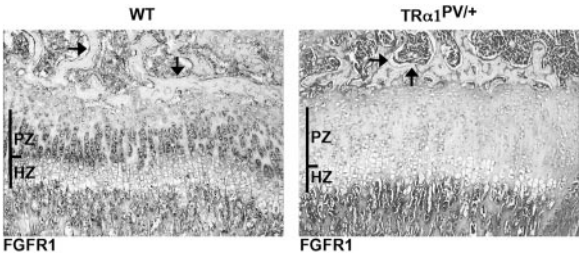

Fig. 7. *In Situ* Hybridizations (×100 Magnification) for FGFR1 in Tibial Growth Plates from 4-wk Wild-Type (WT) and 7-wk TR$\alpha 1^{PV/+}$ Mice

The extent of the PZs and HZs are shown. *Arrows* indicate increased FGFR1 staining in osteoblasts lining trabecular bone surfaces within the secondary epiphysis in WT mice compared with TR$\alpha 1^{PV/+}$ mice.

IGF-IR results in activation of protein kinase B/Akt signaling (24, 25).

The GH/IGF-I pathway was investigated in growth plates from wild-type, TR$\alpha 1^{PV/+}$, TR$\beta^{PV/+}$, and TR$\beta^{PV/PV}$ mice by *in situ* hybridization and immunohistochemistry. In 4-wk wild-type mice, GHR was expressed at low levels only in prehypertrophic chondrocytes at the junction between the PZ and HZ. GHR expression was markedly increased in TR$\beta^{PV/PV}$ mice and extended throughout the PZ, whereas increased expression was also observed in TR$\beta^{PV/+}$ heterozygotes, but this was restricted to prehypertrophic chondrocytes. In contrast, GHR expression was absent from the growth plate in TR$\alpha 1^{PV/+}$ mice, although low levels of expression were evident in immature chondrocytes populating the incompletely formed growth plate from the region of the developing secondary epiphysis (Fig. 8). Low levels of IGF-I expression were also observed in these immature chondrocytes in TR$\alpha 1^{PV/+}$ mice, but not in the growth plate itself. In contrast, there were no differences in levels of IGF-I expression in TR$\beta^{PV/+}$ or TR$\beta^{PV/PV}$ mice compared with wild type, in which IGF-I mRNA was expressed in proliferating chondrocytes (Fig. 8). The patterns of expression of the IGF-IR were similar to those observed for expression of GHR. In wild-type animals IGF-IR was restricted to prehypertrophic chondrocytes. Expression was increased in the same region in TR$\beta^{PV/+}$ heterozygotes but was markedly increased throughout the growth plate in TR$\beta^{PV/PV}$ mice. In the TR$\alpha 1^{PV/+}$, IGF-IR expression was not detected in the growth plate but was present in immature chondrocytes located in the secondary epiphysis (Fig. 8).

To investigate whether the absence of GHR, IGF-I, and IGF-IR expression from growth plates in TR$\alpha 1^{PV/+}$ mice was because of the immaturity of the TR$\alpha 1^{PV/+}$ growth plate, we compared levels of expression in 2-, 3-, and 4-wk-old wild-type, TR$\alpha 1^{PV/+}$, TR$\beta^{PV/+}$, and TR$\beta^{PV/PV}$ mice (Fig. 9 and data not shown). Expression of all three mRNAs was absent from growth plates of TR$\alpha 1^{PV/+}$ mice at all ages but was present at low levels in immature chondrocytes in the region of the secondary epiphysis, consistent with findings in Fig. 8.

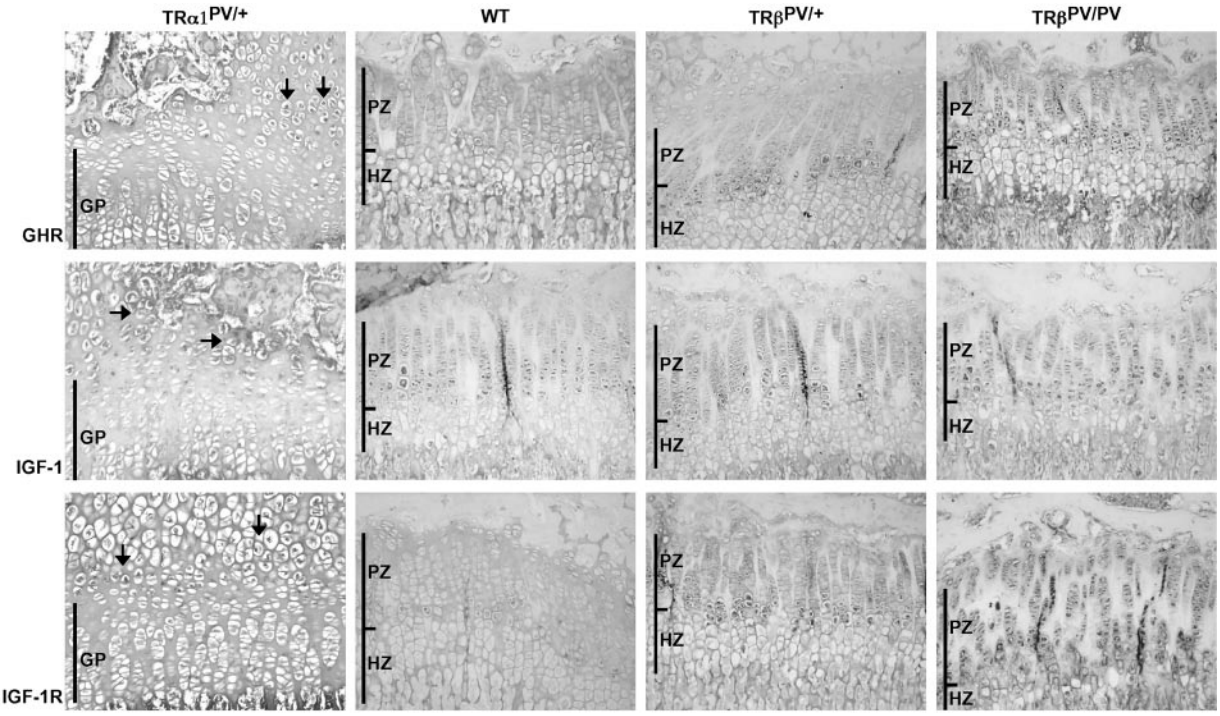

Fig. 8. *In Situ* Hybridizations (×200 Magnification) for GHR, IGF-I, and IGF-IR Expression in Tibial Growth Plates from 4-wk TRα1$^{PV/+}$, Wild-Type (WT), TR$\beta^{PV/+}$ Heterozygote, and TR$\beta^{PV/PV}$ Mice

Note that TR$\beta^{+/+}$ wild-type mice are shown for simplicity; similar data were also obtained from TR$\alpha1^{+/+}$ wild-type mice. The extent of the whole growth plate (GP) and PZs and HZs are shown. *Arrows* indicate positive staining in immature chondrocytes populating the incompletely formed immature growth plate in TRα1$^{PV/+}$ mice.

In wild-type mice, levels of GHR and IGF-IR decreased with age between 2 and 4 wk and became localized to prehypertrophic chondrocytes (Figs. 8 and 9 and data not shown). In contrast, in TR$\beta^{PV/+}$ and TR$\beta^{PV/PV}$ mice, expression of both GHR and IGF-IR remained persistently increased throughout the growth plate at all ages (Figs. 8 and 9 and data not shown). No changes in expression of IGF-I mRNA were observed in wild-type or mutant mice. These data indicate that altered patterns of expression of GHR and IGF-IR mRNAs in TRα1$^{PV/+}$, TR$\beta^{PV/+}$, and TR$\beta^{PV/PV}$ mice are not related to the maturity of the growth plate *per se* and suggest they result from altered skeletal T_3 signaling as a consequence of the TRα1^{PV} or TRβ^{PV} mutation.

To investigate whether changes in mRNA expression correlated with changes in functional activation of GHR and IGF-IR, we investigated the STAT5 and Akt downstream signaling pathways by immunohistochemistry. In TRα1$^{PV/+}$ mice, basal expression of STAT5 and Akt was no different than that of wild type, whereas concentrations of phosphorylated STAT5 and phosphorylated Akt were markedly reduced (Fig. 10). Thus, reduced levels of GHR and IGF-IR mRNAs in TRα1$^{PV/+}$ mice correlated with reduced activation of downstream signaling pathways. In TR$\beta^{PV/+}$ and TR$\beta^{PV/PV}$ mice, levels of basal STAT5 were reduced compared with wild type, whereas levels of basal Akt expression were unchanged. Concentrations of phosphorylated STAT5 and phosphorylated Akt, in contrast, were similar to wild type in TR$\beta^{PV/+}$ mice but were elevated in TR$\beta^{PV/PV}$ mice, although the increase in phosphorylated STAT5 was small (Fig. 11). Thus, increased expression of GHR and IGF-IR mRNAs in TRβ^{PV} mice correlated with increased activation of downstream signaling pathways. Taken together, these data demonstrate that expression and activity of the local growth plate GH/IGF-I signaling pathway is markedly reduced in TRα1^{PV} mice but increased in TRβ^{PV} mice (Table 1), indicating that skeletal thyroid status is a key determinant of the sensitivity of growth plate chondrocytes to the local actions of GH and IGF-I.

DISCUSSION

We have demonstrated that TRα1$^{PV/+}$ mice exhibit a severe 25% reduction in postnatal linear growth, a 3- to 4-wk delay in endochondral ossification, diminished trabecular bone mineralization, reduced cortical bone deposition, and delayed intramembranous ossification. Reduced expression of the T_3-target gene FGFR1 indicates that skeletal hypothyroidism is responsible for this phenotype. The findings contrast with TRβ^{PV} mice, in which skeletal thyrotoxicosis was documented by increased FGFR1 expression, accelerated

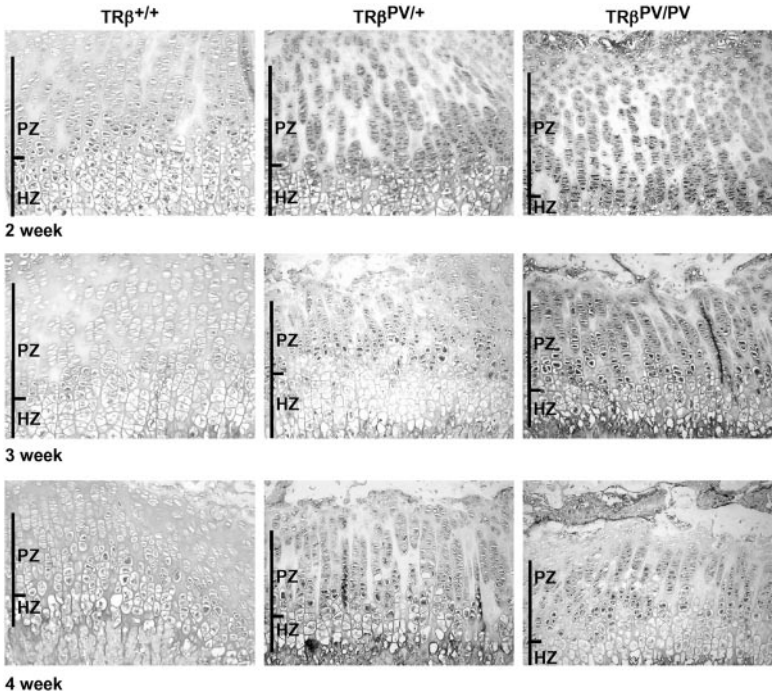

Fig. 9. *In Situ* Hybridizations (×200 Magnification) for IGF-IR Expression in Tibial Growth Plates from 2-, 3-, and 4-wk Wild-Type (TR$\beta^{+/+}$), Heterozygote TR$\beta^{PV/+}$, and TR$\beta^{PV/PV}$ Mice

The extent of the PZs and HZs are shown.

early linear growth, increased trabecular bone mineralization, and advanced endochondral and intramembranous ossification that resulted in short stature and craniosynostosis (13). We previously identified that FGFR1 is a T_3-target gene in bone (19), and the major role of FGFR1 in skeletal development is to regulate intramembranous ossification of the skull (26). Activating mutations of FGFR1 cause Pfeiffer's craniosynostosis syndrome (27), whereas craniosynostosis also occurs in severe childhood thyrotoxicosis (9). The presence of delayed closure of the skull sutures in TRα1$^{PV/+}$ mice, together with craniosynostosis in TR$\beta^{PV/PV}$ mice, suggests FGFR1 mediates important T_3 effects that regulate intramembranous ossification.

Nevertheless, prominent phenotypes in TRα1$^{PV/+}$ and TRβ^{PV} mice involve abnormalities of endochondral bone formation. Thus, we investigated GH and IGF-I signaling in the growth plate, because they are major regulators of endochondral ossification and growth (21, 28, 29). The effects of GH were originally proposed to be mediated by liver-derived IGF-I (30), but this was challenged when IGF-I expression was identified in many tissues (21). A "dual effector theory" for GH action was proposed (31) and extrapolated to the growth plate (32). In this model GH initiates differentiation of PZ chondrocytes directly and is proposed to induce local IGF-I production in proliferating chondrocytes. Local IGF-I then acts in an autocrine/paracrine manner to stimulate clonal expansion and chondrocyte proliferation, resulting in longitudinal growth. However, evidence from IGF-I knockout (IGF-I$^{-/-}$), liver-specific IGF-I knockout (LID), acid-labile subunit knockout (ALSKO) (acid-labile subunit forms a ternary complex with IGF-I and IGF-I binding protein-3 to stabilize serum IGF-I and facilitate its endocrine actions), and LID+ALSKO double-knockout mice have demonstrated that a threshold concentration of circulating IGF-I is also necessary for bone growth. Nevertheless, tissue IGF-I also plays an essential role because IGF-I$^{-/-}$ mice are much more growth retarded than LID+ALSKO double-knockout mice (33–37). Data from GHR knockout (GHR$^{-/-}$), IGF-I$^{-/-}$, and GHR$^{-/-}$IGF-I$^{-/-}$ double mutants indicate that GH and IGF-I act on the growth plate by both independent and overlapping pathways, with IGF-I being the major determinant of embryonic and postnatal growth, and its actions being modulated by GH in the postnatal period (29). It has further been suggested that, because only 17% of somatic growth can be attributed to processes that do not require an intact GH/IGF-I axis, GH and IGF-I pathways in the growth plate act as a point of convergence and participate in the actions of most growth-promoting molecules (29).

This concept is supported by studies showing that IGF-I is stimulated by T_3 in osteoblastic cells (38, 39) and IGF-IR is T_3 responsive in chondrocyte cultures (40). A recent study also showed that T_3 treatment of hypophysectomized rats resulted in increased GHR expression in the growth plate (41), although a previous study showed that GHR expression in the growth plate was independent of thyroid status (42). In addi-

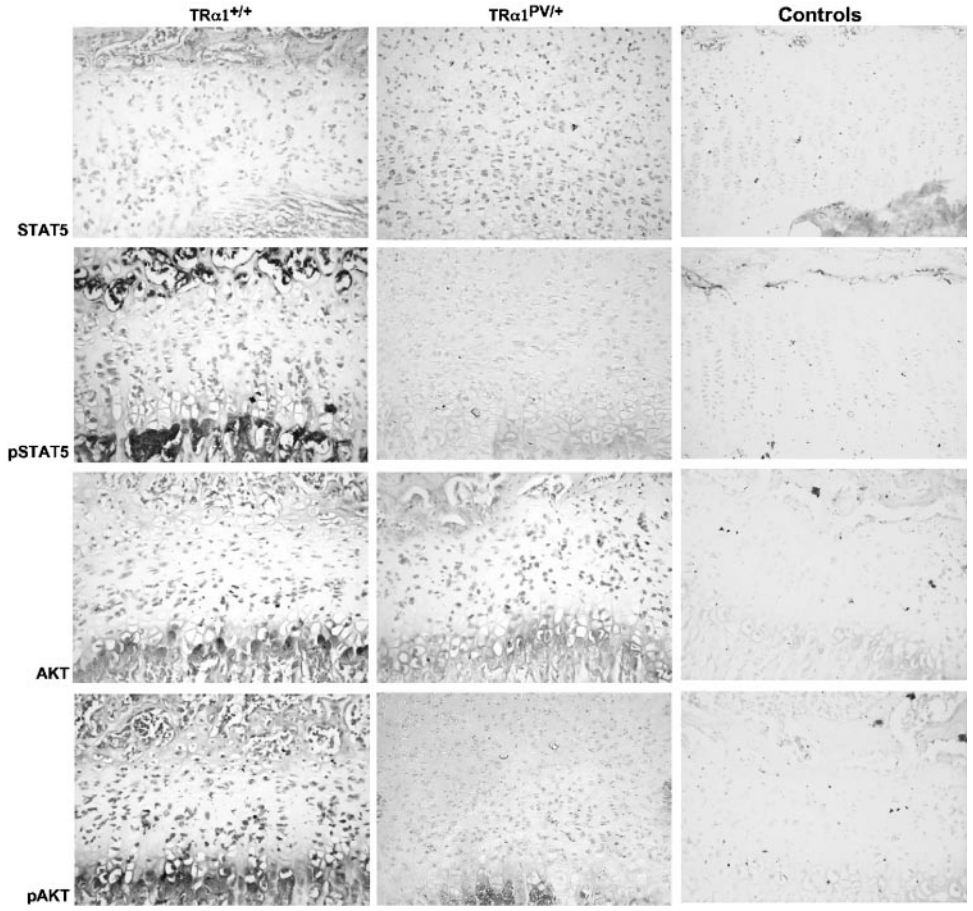

Fig. 10. Immunohistochemistry (×200 Magnification) of STAT5 (*Upper Panels*), pSTAT5 (*Second Row*), Akt (*Third Row*) and pAkt (*Fourth Row*) ProteinExpression in Tibial Growth Plates from Wild-Type (TR$\alpha 1^{+/+}$) and TR$\alpha 1^{PV/+}$ Mice

The *right-hand column* labeled "Controls" shows parallel experiments in which primary antibody was omitted from the immunohistochemistry protocol and which show that staining of STAT and Akt proteins occurred only in the presence specific primary antibody. pSTAT5, Phosphorylated STAT5; pAkt, phosphorylated AKT.

tion to effects on local growth plate GH/IGF-I signaling, T_4 and T_3 influence pituitary GH secretion (43). Abnormalities of the GH/IGF-I axis have been documented in various TR knockout mice: TR$\alpha 1^{-/-\beta-/-}$ mice (which lack TRα1 and TRβ) have GH- and mild IGF-I deficiency (44), and GH replacement restores their growth but does not improve defective ossification (45); TR$\alpha^{0/0\beta-/-}$ mice (lacking all products of the *Thra* and *Thrb* genes) have GH deficiency (17); TR$\alpha^{0/0}$ mice have normal GH production (17); TR$\beta^{-/-}$ mice have mildly reduced GH production (46); and TR$\alpha 2^{-/-}$ mice (which lack TRα2 but overexpress TRα1) have normal GH levels but are IGF-I deficient (47). We previously showed that TR$\alpha 1^{PV/+}$ mice have normal pituitary GH production (15), whereas GH expression is reduced by 80% and circulating IGF-I is reduced by 40% in TR$\beta^{PV/PV}$ mutants (14, 48). These data from various TR mutant mice indicate that T_3, acting mainly via TRβ, regulates systemic GH/IGF-I signaling pathways *in vivo*. Nevertheless, the presence of delayed endochondral ossification in TR$\alpha 1^{PV}$ mice despite normal levels of GH, and the presence of accelerated ossification in TR$\beta^{PV/PV}$ mice in the face of low levels of GH and IGF-I, is discordant with the known actions of GH/IGF-I in the growth plate. These findings strongly suggest that the skeletal consequences of the PV mutation result from dysregulated local GH/IGF-I signaling in the growth plate.

Data in Figs. 8–11 support this by clearly showing that GHR and IGF-IR expression and signaling are reduced in TR$\alpha 1^{PV}$ mice (skeletal hypothyroidism) but increased in TRβ^{PV} mice (skeletal thyrotoxicosis). Nevertheless, the increase in GHR expression in TR$\beta^{PV/PV}$ growth plates (Fig. 8) was accompanied by a disproportionately small rise in activated STAT5 (Fig. 11). This finding reflects the impaired GH production observed in these mice (14) and demonstrates that the net effect of the TRβ^{PV} mutation results from systemic and local consequences on GH action. In contrast, IGF-I expression was unchanged in TR$\beta^{PV/+}$ and TR$\beta^{PV/PV}$ mice compared with wild type and was undetectable in TR$\alpha 1^{PV}$ growth plates, suggesting that TRα and/or GHR activity are necessary for IGF-I expression but indicating that growth plate IGF-I expression is not responsive to increased T_3 or GH action.

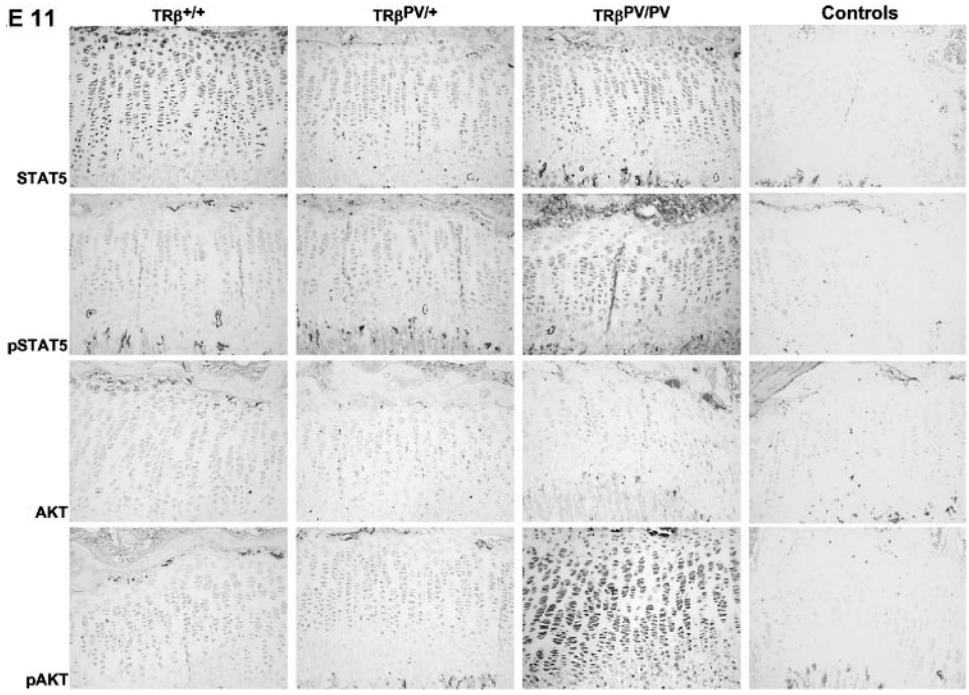

Fig. 11. Immunohistochemistry (×200 Magnification) of STAT5 (*Upper Panels*), pSTAT5 (*Second Row*), Akt (*Third Row*), and pAkt (*Fourth Row*) ProteinExpression in Tibial Growth Plates from Wild-Type ($TR\beta^{+/+}$), $TR\beta^{PV/+}$, and $TR\beta^{PV/PV}$ Mice

The *right-hand column* labeled "controls" shows parallel experiments in which primary antibody was omitted from the immunohistochemistry protocol and which show that staining of STAT and Akt proteins occurred only in the presence of specific primary antibody. pSTAT5, Phosphorylated STAT5; pAkt, phosphorylated AKT.

Nevertheless, increased activation of Akt was observed in $TR\beta^{PV/PV}$ mice and was independent of changes in IGF-I expression, instead correlating with increased IGF-IR expression. These findings suggest that levels of IGF-IR, rather than IGF-I ligand, are limiting in the growth plate. An alternative possibility is that an unidentified T_3-stimulated, IGF-I independent pathway could increase Akt activation in $TR\beta^{PV/PV}$ mice. Taken together, these data indicate that local GH/IGF-I actions mediate important effects of T_3 on endochondral ossification.

Nevertheless, in $TR\alpha1^{PV/+}$ mice with skeletal hypothyroidism and reduced GHR and IGF-IR activity, growth plates were observed to be wider than in wild-type mice (Fig. 4), whereas in $TR\beta^{PV/PV}$ mice, with skeletal thyrotoxicosis and increased GHR and IGF-IR signaling, growth plates were narrower (13). In contrast, growth plates were observed to be narrower in $GHR^{-/-}$ and $IGF\text{-}I^{-/-}$ mice compared with wild type (29, 36, 49), suggesting that T_3 exerts important effects on linear growth that are independent of GH and IGF-I. Indeed, $TR\alpha$ and $TR\beta$ are expressed in growth plate chondrocytes (50–53). T_3 inhibits clonal expansion and proliferation but promotes hypertrophic differentiation of primary chondrocytes in suspension culture (53), and additional studies have shown T_3 regulates the spatial organization of chondrocyte columns and is required for terminal hypertrophic differentiation (54). In contrast, IGF-I stimulates chondrocyte proliferation and differentiation (28). Furthermore, growth retardation in hypothyroidism results from disrupted growth plate architecture, impaired vascular invasion of the growth plate, and inhibition of hypertrophic chondrocyte differentiation (18, 55). Again, differences are apparent as growth retardation in GH and IGF-I deficiency results from a combination of impaired chondrocyte proliferation and a reduction in the linear dimension of terminal hypertrophic chondro-

Table 1. Changes in GH/IGF-I Signaling in $TR\alpha1^{PV}$ and $TR\beta^{PV}$ Mice

	Pituitary GH Production	Growth Plate				
		GHR mRNA	GH Signaling (pSTAT5)	IGF-I mRNA	IGF-IR mRNA	IGF-I Signaling (pAkt)
α1PV	Normal	Reduced	Reduced	Reduced	Reduced	Reduced
βPV	Reduced	Increased	Increased	Normal	Increased	Increased

pSTAT5, Phosphorylated STAT5; pAkt, phosphorylated Akt.

cytes (28, 29, 36, 49, 54). Together, these considerations indicate that regulation of growth and endochondral ossification by T_3 involves both GH/IGF-I-independent and GH/IGF-I-dependent pathways.

In these studies, we showed that TRα1$^{PV/+}$ mice display skeletal hypothyroidism despite the presence of biochemical euthyroidism. In contrast, TRβ^{PV} mice have severe RTH but a phenotype of skeletal thyrotoxicosis (13). This paradox results from differing effects of the PV mutations at the level of the hypothalamic-pituitary-thyroid axis and in bone (Fig. 12). The hypothalamus and pituitary predominantly express TRβ, and mutation or deletion of TRβ results in impaired feedback regulation of TSH and the syndrome of RTH with thyrotoxic levels of T_4 and T_3 and elevated TSH concentrations (14, 44, 46, 56–58). In this situation, the pituitary displays tissue hypothyroidism. In contrast, mutation or deletion of TRα does not interfere significantly with feedback regulation of TSH, and minor changes in circulating T_4 and T_3 levels result from impaired hormone production in the thyroid gland (11, 15–17, 58, 59). In this situation the pituitary functions normally and systemic T_4 and T_3 levels lie within or close to the normal range. Together with data from other mutant mice (reviewed in Refs. 12, 60, and 61), these considerations establish that TRβ is the physiological mediator of negative feedback control of TSH secretion. In contrast, our previous studies suggest that TRα is the major functional TR in bone (13, 17, 19). In the current studies, demonstration of skeletal hypothyroidism and impaired ossification in TRα1$^{PV/+}$ mice establishes that TRα acts directly in bone as a physiological regulator of skeletal development. In this context, it is apparent that the skeletal consequences of disrupted TRβ function in TRβ^{PV} mice result from impaired inhibition of TSH and the resulting elevated T_4 and T_3 concentrations, which act via TRα in bone to induce skeletal thyrotoxicosis (13, 62). In contrast, the skeletal hypothyroidism in TRα1$^{PV/+}$ mice results from locally impaired TRα function in bone.

Our analysis of TRα1$^{PV/+}$ and TRβ^{PV} mice has provided a new understanding of the complex relationship between central pituitary thyroid status and peripheral skeletal thyroid status that arises because the pituitary gland is a TRβ target tissue, whereas bone is a TRα target organ. The model in Fig. 12 can be extended to understand the relationship between central and peripheral thyroid status in any T_3-target tissue, depending on whether the peripheral tissue in question is TRα or TRβ responsive. Thus, in the heart, a TRα-responsive organ, features of thyrotoxicosis are seen in mice with TRβ mutation (63), whereas features of hypothyroidism are seen in TRα mutants (59). In contrast, in the liver, a TRβ target tissue, a hypothyroid phenotype of impaired cholesterol clearance is seen in TRβ mutant mice but not in TRα mutants (64).

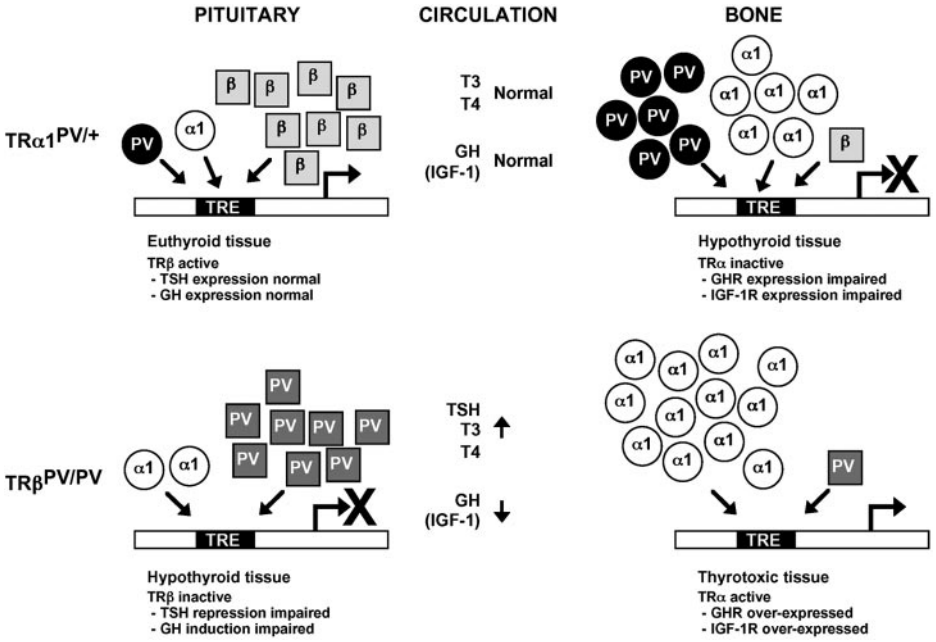

Fig. 12. Relationship between Pituitary and Skeletal Thyroid Status Revealed by Analysis of TRα1$^{PV/+}$ and TR$\beta^{PV/PV}$ Mice

Bone is a TRα-responsive tissue, whereas pituitary is TRβ responsive. The TRα1^{PV} mutation does not affect pituitary T_3 responses because mutant TRα1^{PV} concentrations are too low to interfere with TRβ. In bone, however, T_3 responses are severely impaired because of high concentrations of dominant-negative TRα1^{PV}, resulting in skeletal hypothyroidism. In contrast, the TRβ^{PV} mutation disrupts pituitary T_3 responses and causes RTH, resulting in elevated circulating thyroid hormone concentrations and reduced GH production. In bone, mutant TRβ^{PV} concentrations are too low to interfere with TRα1, and elevated T_4 and T_3 concentrations hyperstimulate TRα1, resulting in skeletal thyrotoxicosis. TRE, Thyroid response element.

MATERIALS AND METHODS

TRα1^{PV} and TRβ^{PV} Mutant Mice

Animal studies were conducted in strict accordance with the National Institutes of Health Guide for Care and Use of Laboratory Animals and were approved by the National Cancer Institute Animal Care and Use Committee. Wild-type, heterozygous (TRα1$^{PV/+}$ and TR$\beta^{PV/+}$), and homozygous (TR$\beta^{PV/PV}$) mutant mice were bred and genotyped as described elsewhere (14, 15). Both TRα1^{PV} and TRβ^{PV} strains were generated from genomic clones isolated from a 129Sv mouse genomic library and transfected into TC-1 embryonic stem cells. Both mutant strains have a mixed C57BL/6J and NIH Black Swiss genetic background. Initial studies have revealed that TRα1$^{PV/+}$ mice exhibit growth retardation with only minor alterations in circulating thyroid hormones (15). In contrast, gross RTH is present in homozygous TR$\beta^{PV/PV}$ mice, with milder thyroid dysfunction in heterozygous TR$\beta^{PV/+}$ mutants (14). Detailed analysis of bone development in TRβ^{PV} mice has revealed accelerated growth, advanced bone age, and short stature resulting from skeletal thyrotoxicosis (13).

Skeletal Preparations

E17.5, P1, P14, P21, P28, and P49 male and female littermate mice were obtained. E17.5 and neonatal mice and limbs from P14, P21, P28, and P49 animals were fixed in 95% ethanol before staining with alizarin red and alcian blue 8GX as described previously (13). Skeletal preparations were photographed using a Leica MZ 75 binocular microscope (Leica AG, Heerbrugg, Switzerland), Leica KL 1500 LCD light source, Leica DFC 320 digital camera, Leica IM50 Digital Image Manager, and Leica Twain Module DFC 320 image acquisition software. Bone lengths from wild-type and TRα1$^{PV/+}$ male and female littermates were determined digitally after linear calibration of pixel size using the image acquisition software. Skull dimensions and open fontanelle and suture areas were calculated using Image J v1.33u software (http://rsb.info.nih.gov/ij/). The assessment of ossification stage in E17.5 and neonatal mice, as determined by the amount of alizarin red staining relative to alcian blue, was more subjective (Fig. 2). In these studies differences that were observed in all mutant mice examined compared with wild-type littermates were considered to be indicative of a difference in the degree of ossification.

Histology

Limbs were fixed for 48–72 h in 10% neutral buffered formalin followed by decalcification in 10% formic acid and 10% neutral buffered formalin at 20 C. E17.5 and P1 limbs were decalcified for 24 h; P14, P21, and P28 limbs were decalcified for 5 d and P49 limbs were decalcified for 7 d. Paraffin-embedded 3-μm sections were taken from anatomically oriented bones (three to five parallel levels per bone depending on the age of the animal; 20 sections per level) and stained with hematoxylin and eosin (Pioneer Research Chemicals, Colchester, UK) or van Gieson and alcian blue 8GX, as described elsewhere (13, 18). Some limbs from E17.5 and P14 mice were also fixed for 48–72 h in 10% neutral buffered formalin and frozen in paraffin without prior decalcification for determination of mineralization by von Kossa staining of 3-μm cryosections with neutral red counterstain (13).

In Situ Hybridization and Analysis of Growth Plate Dimensions

mRNA expression was analyzed in growth plate sections from P14, P21, P28, and P49 mice using collagen II, collagen X, FGFR1, IGF-I, IGF-IR, and GHR cRNA probes. A bacterial neomycin resistance gene cRNA probe (Boehringer Mannheim, Lewes, Sussex, UK) was used as a negative control for all hybridizations, and collagen II (nucleotides 2982–3689; GenBank accession no. L48440) and X (nucleotides 418–858; GenBank accession no. AJ31848) probes were used to identify proliferative and hypertrophic zones in growth plate sections, as described in previous studies in which we optimized *in situ* hybridization methods (13, 18, 19). A rat FGFR1 (nucleotides 104–603; GenBank accession no. S54008) partial cDNA was isolated by RT-PCR as described previously (18, 19) from osteoblastic ROS 17/2.8 cells (65). The rat IGF-I partial cDNA (nucleotides 61–314; GenBank accession no. D00698) was a gift from Dr. Cécile Kedzia (Institut National de la Santé et de la Recherche Médicale, Paris, France). Mouse IGF-1R (nucleotides 1063–1690; GenBank accession no. XM_133508) and GHR (nucleotides 470–711; GenBank accession no. NM_010284) partial cDNAs were isolated by RT-PCR as described elsewhere (18, 19) from chondrogenic ATDC5 cells (66) with the following primers: IGF-1R, forward 5′-GAAGACCACCATCAACAAT-3′, reverse 5′-GAAGGACAAGGAGACCAAG-3′; GHR, forward 5′-GACCCCAGGATCTATTCAGC-3′, reverse 5′-CAGGTTGCACTATTTCGTCAAC-3′. PCR products were subcloned into pGEM-T (Promega, Southampton, Hampshire, UK) and sequenced. FGFR1, IGF-I, IGF-1R, and GHR constructs were linearized with *Spe*I, *Bam*HI, *Dra*II, and *Spe*I, and digoxigenin-labeled cRNA probes were synthesized using T7, T3, T7, and T7 RNA polymerases, respectively (Boehringer Mannheim). *In situ* hybridizations using alkaline phosphatase-labeled probes were performed on 3-μm deparaffinized sections as described elsewhere (13, 18, 19). Studies were performed on at least three mice per genotype in duplicate, and repeat experiments were performed on three separate occasions.

Measurements at four separate positions across the width of growth plates were obtained, using a Leica DM LB2 microscope, Leica DFC 320 digital camera, Leica IM50 Digital Image Manager, and Leica Twain Module DFC 320 image acquisition software, to calculate mean values for the heights of the RZ, PZ, HZ, and total growth plate in sections from wild-type and TRα1$^{PV/+}$ mice. Results from adjacent levels of sectioning were compared to ensure consistency of the data. Cortical bone width measurements were performed at four separate positions in the midshaft of the tibia and adjacent levels of sectioning were compared. All studies are performed with the observer blinded to the genotype. For histology and histomorphometry analyses, at least three animals per genotype were examined.

Immunohistochemistry

Activation of IGF-IR and GHR downstream signaling was examined by immunohistochemical analysis of protein kinase B (Akt) and signal transducer and activator of transcription-5 (STAT5) expression in wild-type, TRα1$^{PV/+}$, TR$\beta^{PV/+}$, and TR$\beta^{PV/PV}$ growth plates. Sections were deparaffinized and rehydrated in ethanol and PBS. Sodium citrate antigen retrieval was performed for 6 min in a microwave oven on medium setting. Endogenous peroxidase activity was quenched with 1% H_2O_2 in methanol for 15 min at room temperature. Sections were then blocked with 5% fetal calf serum (Sigma Chemical Co., St. Louis, MO) in PBS with 0.5% Tween 20 for 1 h at room temperature, before addition of primary antibody and incubation overnight at 4 C. Polyclonal antibodies used to detect expression of Akt (Santa Cruz Biotechnology. Inc., Santa Cruz, CA), phosphorylated Akt (Cell Signaling Technology, Inc., Beverly, MA), STAT5 (Santa Cruz), and phosphorylated STAT5 (Santa Cruz) were diluted 1:175, 1:50, 1:200, and 1:140, respectively. Sections were subsequently incubated with peroxidase-conjugated secondary antibody (Bio-Rad Laboratories, Inc., Hercules, CA) diluted 1:2000 to 1:1800 for 30 min at room temperature. Peroxidase activity was detected using 3,3′-diaminobenzi-

dine containing 0.02% H_2O_2 (Sigma). Negative controls lacking primary antibody were performed in parallel in all experiments, as described elsewhere (53, 67). Studies were performed on at least three mice per genotype in duplicate, and repeat experiments were performed on three separate occasions.

Statistical Analysis

Data were expressed as mean ± SEM. Differences between groups were examined for statistical significance using Student's *t* test, in which *P* values <0.05 were considered significant.

Acknowledgments

Received June 8, 2005. Accepted July 20, 2005.

Address all correspondence and requests for reprints to: Graham R. Williams, Molecular Endocrinology Group, 5th Floor Clinical Research Building, Medical Research Council Clinical Sciences Centre, Hammersmith Hospital, Du Cane Road, London W12 0NN, United Kingdom. E-mail: graham.williams@imperial.ac.uk

This work was supported by a Medical Research Council (MRC) Ph.D./Studentship (to P.J.O'S.), MRC Clinician Scientist Fellowship (to J.H.D.B.), and MRC Career Establishment Grant (G9803002) (to G.R.W.).

REFERENCES

1. Cheng SY 2000 Multiple mechanisms for regulation of the transcriptional activity of thyroid hormone receptors. Rev Endocr Metab Disord 1:9–18
2. Forrest D, Sjoberg M, Vennstrom B 1990 Contrasting developmental and tissue-specific expression of α and β thyroid hormone receptor genes. EMBO J 9:1519–1528
3. Williams GR 2000 Cloning and characterization of two novel thyroid hormone receptor β isoforms. Mol Cell Biol 20:8329–8342
4. Murphy E, Williams GR 2004 The thyroid and the skeleton. Clin Endocrinol (Oxf) 61:285–298
5. Harvey CB, O'Shea PJ, Scott AJ, Robson H, Siebler T, Shalet M, Samrut J, Chassande O, Williams GR 2002 Molecular mechanisms of thyroid hormone effects on bone growth and function. Mol Genet Metab 75:17–30
6. Rivkees SA, Bode HH, Crawford JD 1988 Long-term growth in juvenile acquired hypothyroidism: the failure to achieve normal adult stature. N Engl J Med 318:599–602
7. Weiss RE, Refetoff S 1996 Effect of thyroid hormone on growth. Lessons from the syndrome of resistance to thyroid hormone. Endocrinol Metab Clin North Am 25: 719–730
8. Kvistad PH, Lovas K, Boman H, Myking OL 2004 Retarded bone growth in thyroid hormone resistance. A clinical study of a large family with a novel thyroid hormone receptor mutation. Eur J Endocrinol 150:425–430
9. Segni M, Leonardi E, Mazzoncini B, Pucarelli I, Pasquino AM 1999 Special features of Graves' disease in early childhood. Thyroid 9:871–877
10. Weiss RE, Refetoff S 2000 Resistance to thyroid hormone. Rev Endocr Metab Disord 1:97–108
11. Tinnikov A, Nordstrom K, Thoren P, Kindblom JM, Malin S, Rozell B, Adams M, Rajanayagam O, Pettersson S, Ohlsson C, Chatterjee K, Vennstrom B 2002 Retardation of post-natal development caused by a negatively acting thyroid hormone receptor α1. EMBO J 21:5079–5087
12. O'Shea PJ, Williams GR 2002 Insight into the physiological actions of thyroid hormone receptors from genetically modified mice. J Endocrinol 175:553–570
13. O'Shea PJ, Harvey CB, Suzuki H, Kaneshige M, Kaneshige K, Cheng SY, Williams GR 2003 A thyrotoxic skeletal phenotype of advanced bone formation in mice with resistance to thyroid hormone. Mol Endocrinol 17: 1410–1424
14. Kaneshige M, Kaneshige K, Zhu X, Dace A, Garrett L, Carter TA, Kazlauskaite R, Pankrantz DG, Wynshaw-Boris A, Refetoff S, Weintraub B, Willingham MC, Barlow C, Cheng S 2000 Mice with a targeted mutation in the thyroid hormone β receptor gene exhibit impaired growth and resistance to thyroid hormone. Proc Natl Acad Sci USA 97:13209–13214
15. Kaneshige M, Suzuki H, Kaneshige K, Cheng J, Wimbrow H, Barlow C, Willingham MC, Cheng S 2001 A targeted dominant negative mutation of the thyroid hormone α 1 receptor causes increased mortality, infertility, and dwarfism in mice. Proc Natl Acad Sci USA 98: 15095–15100
16. Liu YY, Schultz JJ, Brent GA 2003 A thyroid hormone receptor α gene mutation (P398H) is associated with visceral adiposity and impaired catecholamine-stimulated lipolysis in mice. J Biol Chem 278:38913–38920
17. Gauthier K, Plateroti M, Harvey CB, Williams GR, Weiss RE, Refetoff S, Willott JF, Sundin V, Roux JP, Malaval L, Hara M, Samurut J, Chassande O 2001 Genetic analysis reveals different functions for the products of the thyroid hormone receptor α locus. Mol Cell Biol 21:4748–4760
18. Stevens DA, Hasserjian RP, Robson H, Siebler T, Shalet SM, Williams GR 2000 Thyroid hormones regulate hypertrophic chondrocyte differentiation and expression of parathyroid hormone-related peptide and its receptor during endochondral bone formation. J Bone Miner Res 15:2431–2442
19. Stevens DA, Harvey CB, Scott AJ, O'Shea PJ, Barnard JC, Williams AJ, Brady G, Samurut J, Chassande O, Williams GR 2003 Thyroid hormone activates fibroblast growth factor receptor-1 in bone. Mol Endocrinol 17: 1751–1766
20. Lefebvre V, Huang W, Harley VR, Goodfellow PN, de Crombrugghe B 1997 SOX9 is a potent activator of the chondrocyte-specific enhancer of the pro α1(II) collagen gene. Mol Cell Biol 17:2336–2346
21. Butler AA, Le Roith D 2001 Control of growth by the somatropic axis: growth hormone and the insulin-like growth factors have related and independent roles. Annu Rev Physiol 63:141–164
22. Piwien-Pilipuk G, Huo JS, Schwartz J 2002 Growth hormone signal transduction. J Pediatr Endocrinol Metab 15:771–786
23. Teglund S, McKay C, Schuetz E, van Deursen JM, Stravopodis D, Wang D, Brown M, Bodner S, Grosveld G, Ihle JN 1998 Stat5a and Stat5b proteins have essential and nonessential, or redundant, roles in cytokine responses. Cell 93:841–850
24. Vincent AM, Feldman EL 2002 Control of cell survival by IGF signaling pathways. Growth Horm IGF Res 12: 193–197
25. Peng XD, Xu PZ, Chen ML, Hahn-Windgassen A, Skeen J, Jacobs J, Sundarajan D, Chen WS, Crawford SE, Coleman KG, Hay N 2003 Dwarfism, impaired skin development, skeletal muscle atrophy, delayed bone development, and impeded adipogenesis in mice lacking Akt1 and Akt2. Genes Dev 17:1352–1365
26. Ornitz DM, Marie PJ 2002 FGF signaling pathways in endochondral and intramembranous bone development and human genetic disease. Genes Dev 16:1446–1465
27. Muenke M, Schell U, Hehr A, Robin NH, Losken HW, Schinzel A, Pulleyn LJ, Rutland P, Reardon W, Malcolm S, Winter RM 1994 A common mutation in the fibroblast growth factor receptor 1 gene in Pfeiffer syndrome. Nat Genet 8:269–274

28. van der Eerden BC, Karperien M, Wit JM 2003 Systemic and local regulation of the growth plate. Endocr Rev 24:782–801
29. Lupu F, Terwilliger JD, Lee K, Segre GV, Efstratiadis A 2001 Roles of growth hormone and insulin-like growth factor 1 in mouse postnatal growth. Dev Biol 229: 141–162
30. Salmon Jr WD, Daughaday WH 1957 A hormonally controlled serum factor which stimulates sulfate incorporation by cartilage in vitro. J Lab Clin Med 49:825–836
31. Green H, Morikawa M, Nixon T 1985 A dual effector theory of growth-hormone action. Differentiation 29: 195–198
32. Isaksson OG, Lindahl A, Nilsson A, Isgaard J 1987 Mechanism of the stimulatory effect of growth hormone on longitudinal bone growth. Endocr Rev 8:426–438
33. Baker J, Liu JP, Robertson EJ, Efstratiadis A 1993 Role of insulin-like growth factors in embryonic and postnatal growth. Cell 75:73–82
34. Liu JP, Baker J, Perkins AS, Robertson EJ, Efstratiadis A 1993 Mice carrying null mutations of the genes encoding insulin-like growth factor I (Igf-1) and type 1 IGF receptor (Igf1r). Cell 75:59–72
35. Powell-Braxton L, Hollingshead P, Warburton C, Dowd M, Pitts-Meek S, Dalton D, Gillett N, Stewart TA 1993 IGF-I is required for normal embryonic growth in mice. Genes Dev 7:2609–2617
36. Yakar S, Rosen CJ, Beamer WG, Ackert-Bicknell CL, Wu Y, Liu JL, Ooi GT, Setser J, Frystyk J, Boisclair YR, LeRoith D 2002 Circulating levels of IGF-1 directly regulate bone growth and density. J Clin Invest 110:771–781
37. Yakar S, Kim H, Zhao H, Toyoshima Y, Pennisi P, Gavrilova O, Leroith D 2005 The growth hormone-insulin like growth factor axis revisited: lessons from IGF-1 and IGF-1 receptor gene targeting. Pediatr Nephrol 20: 251–254
38. Lakatos P, Caplice MD, Khanna V, Stern PH 1993 Thyroid hormones increase insulin-like growth factor I content in the medium of rat bone tissue. J Bone Miner Res 8:1475–1481
39. Varga F, Rumpler M, Klaushofer K 1994 Thyroid hormones increase insulin-like growth factor mRNA levels in the clonal osteoblastic cell line MC3T3-E1. FEBS Lett 345:67–70
40. Ohlsson C, Nilsson A, Isaksson O, Bentham J, Lindahl A 1992 Effects of tri-iodothyronine and insulin-like growth factor-I (IGF-I) on alkaline phosphatase activity, [^{3}H]thymidine incorporation and IGF-I receptor mRNA in cultured rat epiphyseal chondrocytes. J Endocrinol 135: 115–123
41. Gevers EF, van der Eerden BC, Karperien M, Raap AK, Robinson IC, Wit JM 2002 Localization and regulation of the growth hormone receptor and growth hormone-binding protein in the rat growth plate. J Bone Miner Res 17:1408–1419
42. Lewinson D, Bialik GM, Hochberg Z 1994 Differential effects of hypothyroidism on the cartilage and the osteogenic process in the mandibular condyle: recovery by growth hormone and thyroxine. Endocrinology 135: 1504–1510
43. Ohlsson C, Bengtsson BA, Isaksson OG, Andreassen TT, Slootweg MC 1998 Growth hormone and bone. Endocr Rev 19:55–79
44. Gothe S, Wang Z, Ng L, Kindblom JM, Barros AC, Ohlsson C, Vennstrom B, Forrest D 1999 Mice devoid of all known thyroid hormone receptors are viable but exhibit disorders of the pituitary-thyroid axis, growth, and bone maturation. Genes Dev 13:1329–1341
45. Kindblom JM, Gothe S, Forrest D, Tornell J, Vennstrom B, Ohlsson C 2001 GH substitution reverses the growth phenotype but not the defective ossification in thyroid hormone receptor $\alpha 1-/-\beta-/-$ mice. J Endocrinol 171: 15–22
46. Forrest D, Hanebuth E, Smeyne RJ, et al 1996 Recessive resistance to thyroid hormone in mice lacking thyroid hormone receptor β: evidence for tissue-specific modulation of receptor function. EMBO J 15:3006–3015
47. Salto C, Kindblom JM, Johansson C, Wang Z, Gullberg H, Nordstrom K, Mansen A, Ohlsson C, Thoren P, Forrest D, Vennstrom B 2001 Ablation of TRα2 and a concomitant overexpression of α1 yields a mixed hypo- and hyperthyroid phenotype in mice. Mol Endocrinol 15: 2115–2128
48. Suzuki H, Cheng SY 2003 Compensatory role of thyroid hormone receptor (TR) α 1 in resistance to thyroid hormone: study in mice with a targeted mutation in the TR β gene and deficient in TR α 1. Mol Endocrinol 17: 1647–1655
49. Sims NA, Clement-Lacroix P, Da Ponte F, Bouali Y, Binart N, Moriggl R, Goffin V, Coschigano K, Gaillard-Kelly M, Kopchick J, Baron R, Kelly PA 2000 Bone homeostasis in growth hormone receptor-null mice is restored by IGF-I but independent of Stat5. J Clin Invest 106: 1095–1103
50. Abu EO, Bord S, Horner A, Chatterjee VK, Compston JE 1997 The expression of thyroid hormone receptors in human bone. Bone 21:137–142
51. Ballock R, Mita BC, Zhou X, Chen DH, Mink LM 1999 Expression of thyroid hormone receptor isoforms in rat growth plate cartilage in vivo. J Bone Miner Res 14: 1550–1556
52. Carrascosa A, Ferrandez MA, Audi L, Ballabriga A 1992 Effects of triiodothyronine (T_3) and identification of specific nuclear T_3-binding sites in cultured human fetal epiphyseal chondrocytes. J Clin Endocrinol Metab 75: 140–144
53. Robson H, Siebler T, Stevens DA, Shalet SM, Williams GR 2000 Thyroid hormone acts directly on growth plate chondrocytes to promote hypertrophic differentiation and inhibit clonal expansion and cell proliferation. Endocrinology 141:3887–3897
54. Robson H, Siebler T, Shalet SM, Williams GR 2002 Interactions between GH, IGF-I, glucocorticoids, and thyroid hormones during skeletal growth. Pediatr Res 52: 137–147
55. Lewinson D, Harel Z, Shenzer P, Silbermann M, Hochberg Z 1989 Effect of thyroid hormone and growth hormone on recovery from hypothyroidism of epiphyseal growth plate cartilage and its adjacent bone. Endocrinology 124:937–945
56. Abel ED, Moura EG, Ahima RS, Campos-Barros A, Pazos-Moura CC, Boers ME, Kaulbach HC, Forrest D, Wondisford FE 2003 Dominant inhibition of thyroid hormone action selectively in the pituitary of thyroid hormone receptor-β null mice abolishes the regulation of thyrotropin by thyroid hormone. Mol Endocrinol 17: 1767–1776
57. Abel ED, Kaulbach HC, Campos-Barros A, Ahima RS, Boers ME, Hashimoto K, Forrest D, Wondisford FE 1999 Novel insight from transgenic mice into thyroid hormone resistance and the regulation of thyrotropin. J Clin Invest 103:271–279
58. Gauthier K, Chassande O, Plateroti M, Roux JP, Legrand C, Pain B, Rousset B, Weiss R, Trouillas J, Samurut J 1999 Different functions for the thyroid hormone receptors TRα and TRβ in the control of thyroid hormone production and post-natal development. EMBO J 18: 623–631
59. Wikstrom L, Johansson C, Salto C, Barlow C, Campos Barros A, Baas, F, Forrest D, Thoren P, Vennstrom B 1998 Abnormal heart rate and body temperature in mice lacking thyroid hormone receptor α 1. EMBO J 17: 455–461
60. Flamant F, Samarut J 2003 Thyroid hormone receptors: lessons from knockout and knock-in mutant mice. Trends Endocrinol Metab 14:85–90

61. Forrest D, Vennstrom B 2000 Functions of thyroid hormone receptors in mice. Thyroid 10:41–52
62. Zhang XY, Kaneshige M, Kamiya Y, Kaneshige K, McPhie P, Cheng SY 2002 Differential expression of thyroid hormone receptor isoforms dictates the dominant negative activity of mutant β receptor. Mol Endocrinol 16:2077–2092
63. Gloss B, Trost S, Bluhm W, Swanson E, Clark R, Winkfein R, Janzen K, Giles W, Chassande O, Samurut J, Dillman W 2001 Cardiac ion channel expression and contractile function in mice with deletion of thyroid hormone receptor α or β. Endocrinology 142:544–550
64. Gullberg H, Rudling M, Salto C, Forrest D, Angelin B, Vennstrom B 2002 Requirement for thyroid hormone receptor β in T_3 regulation of cholesterol metabolism in mice. Mol Endocrinol 16:1767–1777
65. Williams GR, Bland R, Sheppard MC 1994 Characterization of thyroid hormone (T_3) receptors in three osteosarcoma cell lines of distinct osteoblast phenotype: interactions among T_3, vitamin D_3, and retinoid signaling. Endocrinology 135:2375–2385
66. Shukunami C, Shigeno C, Atsumi T, Ishizeki K, Suzuki F, Hiraki Y 1996 Chondrogenic differentiation of clonal mouse embryonic cell line ATDC5 in vitro: differentiation-dependent gene expression of parathyroid hormone (PTH)/PTH-related peptide receptor. J Cell Biol 133: 457–468
67. Siebler T, Robson H, Bromley M, Stevens DA, Shalet SM, Williams GR 2002 Thyroid status affects number and localization of thyroid hormone receptor expressing mast cells in bone marrow. Bone 30:259–266

Molecular Endocrinology **is published monthly by The Endocrine Society (http://www.endo-society.org), the foremost professional society serving the endocrine community.**

Geoffrey Harris Prize in Neuroendocrinology

We are pleased to announce the 2006 Geoffrey Harris Prize, generously sponsored by Ipsen. This important prize, worth 12,000 Euros, is designed for established researchers in the field of neuroendocrinology and is the first of its kind in Europe. Please contact the EFES/ESE Secretary:

Professor Philippe Bouchard
Service d'Endocrinologie
Hôpital Saint Antoine
184 rue du Faubourg Saint Antoine
75012 Paris, France
E-mail: philippe.bouchard@sat.ap-hop-paris.fr

The deadline for entries is **31 December 2005**, and the award will be presented at the 8th European Congress of Endocrinology, which takes place from 1-4 April 2006 in Glasgow, UK. The winner will be asked to give one of the main lectures, in addition to two other lectures at future EFES/ESE scientific meetings.

For more information about the prize and details on application, please go to http://www.euro-endo.org/about/harrisprize.htm